



Calcareous nannofossils identify the age and precipitation rates of manganese deposits of the Mozambique Ridge and Mozambique Basin, SW Indian Ocean

M. N. Ovechkina^{1,2} · M. K. Watkeys² · M. B. Mostovski^{3,4} · W. Kretzinger² · S. M. Perritt⁵

Received: 14 January 2021 / Accepted: 15 June 2021 / Published online: 17 July 2021
© The Author(s), under exclusive licence to Springer-Verlag GmbH Germany, part of Springer Nature 2021

Abstract

Calcareous nannofossil assemblages identified in manganese deposits dredged at three sites on the Mozambique Ridge and one on the Jaguar seamount in the Mozambique Basin comprise 61 species, including nine reworked ones. The samples represent cores of nodules or encrustations ranging from 4.04 to 0.00 Ma. Dating by nannofossils suggests bi-modal ages for the samples, the late Zanclean–Piacenzian (Pliocene) and the Calabrian (Pleistocene)–Holocene. The calculated rates of manganese precipitation range from 4.7 to 248.3 mm/Ma, which are generally typical for hydrothermal manganese accretion. The bi-modal age distribution points to oceanographic changes during the Pliocene–Holocene. The Pliocene manganese precipitation may reflect the closing of the Panama Isthmus, while the terminal Pleistocene–Holocene accretion may result from oceanic fluctuations caused by glacial and interglacial periods. Fe–Mn oxide precipitation rates at the Makarov Guyot, NW Pacific, re-calculated on the basis of the most recent calcareous nannofossil biostratigraphy, suggest hydrothermal processes of manganese accretion in that part of the West Pacific Seamount Province.

Keywords Calcareous nannoplankton · Coccoliths · Cenozoic · Tertiary · Quaternary · Biostratigraphy · Fe–Mn oxide precipitation · Hydrothermal manganese accretion · Mozambique Channel · South Africa

This article is part of the Topical Collection on *Coastal and marine geology in Southern Africa: alluvial to abyssal and everything in between*

✉ M. N. Ovechkina
mariao@gsi.gov.il

✉ M. B. Mostovski
mike.mostovski@gmail.com

¹ Geological Survey of Israel, Yesha'yahu Leibowitz 32, 9692100 Jerusalem, Israel

² School of Agricultural, Earth and Environmental Sciences, University of KwaZulu-Natal, Durban, South Africa

³ The Steinhardt Museum of Natural History, Israel National Center for Biodiversity Studies, Tel Aviv University, 69978 Tel Aviv, Israel

⁴ School of Life Sciences, University of KwaZulu-Natal, P. Bag X01, Scottsville 3209, South Africa

⁵ Council for Scientific and Industrial Research, Johannesburg, South Africa

Introduction

Iron-manganese (Fe–Mn) oxide crusts and nodules ('manganese nodules') cover substantial areas of the global seafloor, attract considerable quantities of trace and rare earth elements due to their properties and slow accumulation rates (Koschinsky and Hein 2017), and are considered as a potential ore source for rare metals (Hein et al. 2013). Multidisciplinary approaches have been employed, especially in recent years, to understand oceanographic factors that influence spatial distribution and growth rates of Fe–Mn oxide crusts and nodules (e.g. Shkolnik et al. 2012; Josso et al. 2019, 2020; Benites et al. 2020; Charles et al. 2020). Fe–Mn oxide encrustations can be of different geochemical origin (Koschinsky and Hein 2017), although bacteria and even coccolithophores also play an important role in initiation and development of Fe–Mn oxide deposition (e.g. Wang and Müller 2009; Wang et al. 2011; Shkolnik et al. 2012; Jiang et al. 2019). Most work on dating Fe–Mn oxide crusts and nodules has been done based on trace and rare earth element isotopes and radiometric techniques (Josso et al. 2019, 2020, and references cited therein), but calcareous nannofossils

have also been used to estimate the age of polymetallic concretions (Janin 1985, 1987) and the growth rates of ferromanganese nodules and crusts (Harada and Nishida 1976; Cowen et al. 1993) in the North-West and Central Pacific.

Very little work has been done on understanding Fe–Mn oxide deposition in SW Indian Ocean and, in particular, off South Africa and in the Mozambique Channel (Rogers 1995; Albarède et al. 1997; Frank et al. 2002; Charles et al. 2020).

During the SO-183 cruise of the RV Sonne (Jokat 2006), dredging of the Mozambique Ridge and in the Mozambique Basin resulted in the collection of a suite of manganese nodules, rocks encased by manganese encrustations, and individual manganese encrustations (Watkeys et al. 2006). Geochemical analyses of these samples, combined with previous data from the region, revealed that the manganese mineralisation was formed primarily by hydrogenetic processes, with secondary diagenetic enrichment having taken place on the Mozambique Ridge crest and possibly some hydrothermal enrichment on the Ridge flanks (Perritt and Watkeys 2007).

This paper reports on the calcareous nannofossils from the manganese nodules and encrustations of the Mozambique Ridge and in the Mozambique Basin. This provides the first model for establishing both the age and rate of Fe–Mn oxide precipitation in the SW Indian Ocean using micropalaeontological data and allows the genesis of these nodules and encrustations to be linked to major changes in oceanographic conditions and tectonic activity in the region during the late Cenozoic.

Materials and methods

The calcareous nannofossil assemblages come from samples collected from three localities (DL1, DL2, DL3) on the Mozambique Ridge and one (DL4) on the Jaguar seamount in the Mozambique Basin (Fig. 1, Table 1). The sites are up to 1500 km apart and range in depths from 4077 to 756 m. At all but one site, two dredges were undertaken. The dredging methodology was described by Watkeys et al. (2006).

Dredge samples of manganese nodules and encrustations were cut on-board the RV Sonne and examined under a binocular microscope. This revealed the presence of calcareous centres to manganese nodules, recorded as chalk cores, and thin calcareous layers at the base of and within the manganese encrustations (Watkeys et al. 2006). It was suspected that these layers contained calcareous nannofossils, which are a very useful tool for establishing the age of sediments, especially when only very small quantities of sediments are available for analysis (Bosman et al. 2007). In the laboratory on-shore, a standard technique of nannofossil identification was used for the preparation of the smear slides (Green et al. 2008). Totally 30 samples were analysed under a light microscope Olympus BX53 at 1250× magnification with

phase contrast and cross-polarised light. Photographs are taken with an Olympus digital camera (Fig. 2). Scanning electron microscopy (SEM) was employed to confirm identifications and for photographing biostratigraphically important species (Fig. 3).

The abbreviations FO and LO are used for the first known occurrence and the last known occurrence of the nannofossil species in the geological record.

Abundance of individual calcareous nannofossil taxa is recorded as follows:

- A—abundant (> 10 specimens per field of view (FOV));
- C—common (> 1–10 specimens per FOV);
- F—few (1 specimen per 1–10 FOV);
- R—rare (< 1 specimen per 10 FOV);
- VR—very rare (1 specimen per slide).

Nannofossil preservation has been determined based on following criteria:

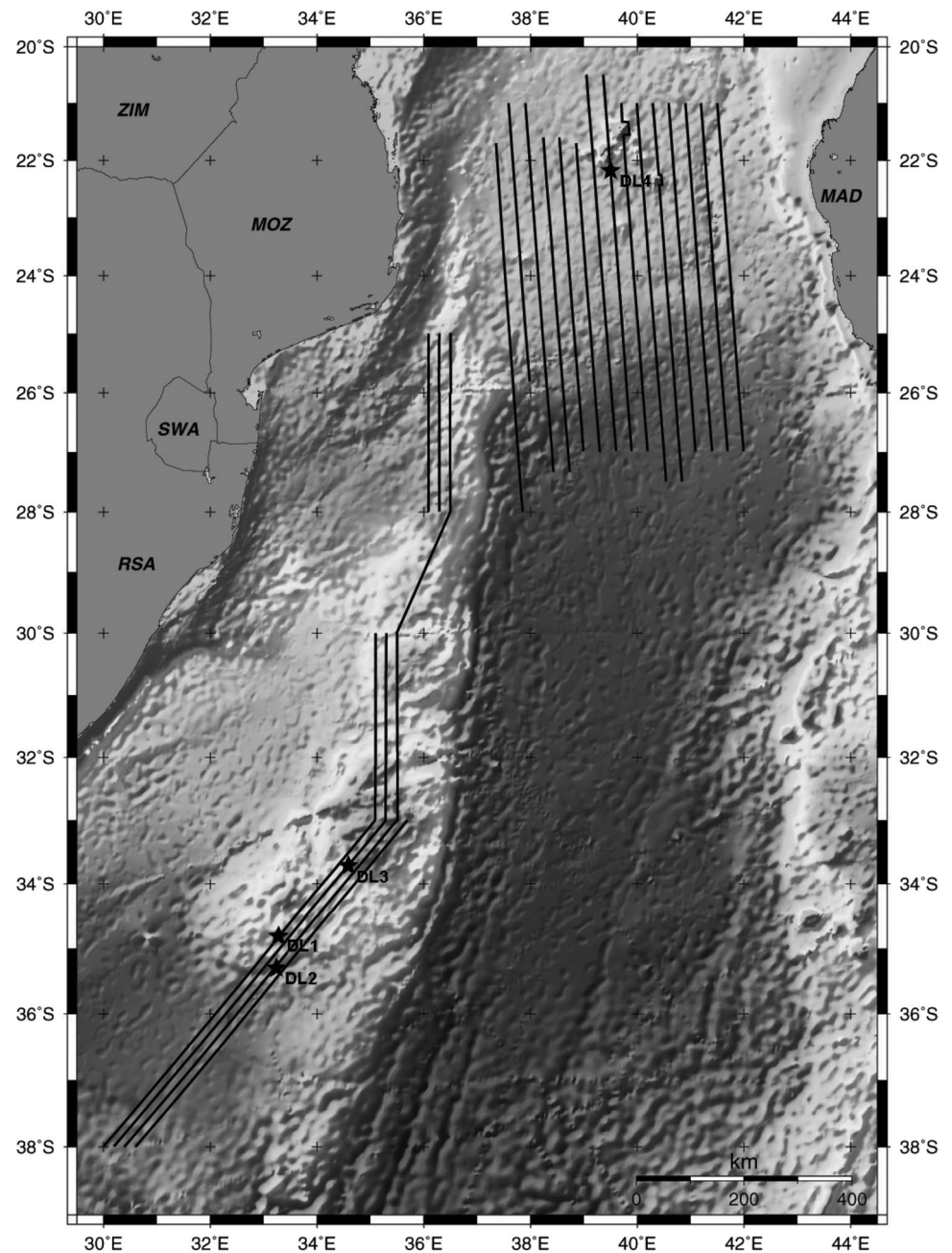
- G—good, most specimens exhibit little or no secondary alteration, little or no evidence of dissolution and/or recrystallization;
- M—moderate, all specimens are easily identifiable to the species level, but exhibit some etching and/or recrystallization from calcite dissolution and/or overgrowth;
- P—poor, identification of species is hampered at the species and/or generic level but possible in some cases; specimens are severely etched or overgrown, primary morphological characteristics are largely destroyed and fragmentation occurs.

The overall preservation of the nannofossils is good, except for dredge site DL2. Here, the samples were collected at about 3.5–4.0 km depth, which is close to the carbonate compensation depth (CCD) (Perritt and Watkeys 2007). Consequently, the poor preservation of the calcareous nannofossils is not unexpected.

Taxonomy of the calcareous nannofossil species follows Perch-Nielsen (1985), Rio et al. (1990), Sato and Takayama (1992), Young and Bown (1997), Bown (2005) and Young et al. (2017). Identification of the genus *Gephyrocapsa* has been based on the measurements provided by Backman et al. (2012) for *gephyrocapsid* placoliths: ‘small sized’, < 4.0 µm; ‘medium sized’, 4.0–5.5 µm (*Gephyrocapsa* spp. ≥ 4 µm in the zonation of Backman et al. (2012)) and ‘large sized’, > 5.5 µm.

For biostratigraphic interpretations of the samples by calcareous nannofossils, standard zonations by Martini (1971) and Okada and Bukry (1980) and a new scheme of Backman et al. (2012) have been applied. The combination of schemes by Martini (1971) and Backman et al. (2012) provides a better age constrain for the studied samples.

Fig. 1 Map of the Mozambique Ridge and environs with sample sites. The lines show the course of the ship, along which dredging was carried. The map is modified after König and Jokát (2010)



The minimum growth rate of Mn encrustations has been calculated as a range, using the earliest and latest possible datings provided by calcareous nannofossils. The age of calcareous nannofossil zonal boundaries is given after Gradstein et al. (2020).

Results

Preliminary biostratigraphic results were published elsewhere (Ovechkina et al. 2009). Out of 30 examined samples, 21 samples contained representative assemblages of

nannoplankton, which included 61 species, with nine species being reworked (Appendix); the other samples were barren. The preservation of nannofossils is generally good and moderate.

Dredge locality DL1

This locality, which is towards the southern end of the Mozambique Ridge (Fig. 1; Table 1), yielded some mafic igneous rocks encrusted by manganese but the samples largely comprised encrustations only. The surfaces of some samples were covered in small black nodules approximately

Table 1 Summary of dredge localities

Locality	Dredge	Latitude, S	Longitude, E	Depth, m
DL1	On bottom	34°48'52"	33°17'27"	2699
	Off bottom	34°48'15"	33°17'62"	2461
	On bottom	34°48'58"	33°17'21"	2725
	Off bottom	34°48'04"	33°17'78"	2440
DL2	On bottom	35°18'53"	33°14'45"	4077
	Off bottom	35°17'53"	33°14'16"	3526
	On bottom	35°18'37"	33°14'23"	3932
	Off bottom	35°17'06"	33°13'62"	3508
DL3	On bottom	33°41'16"	34°36'14"	1898
	Off bottom	33°40'52"	34°36'51"	1804
DL4	On bottom	21°56'48"	39°28'71"	1111
	Off bottom	21°56'46"	39°28'57"	984
	On bottom	21°56'47"	39°28'67"	1097
	Off bottom	21°56'23"	39°28'32"	756

1 mm in diameter, typical of manganese growth on a surface exposed to ocean water. The encrustations exhibit very fine laminations, which are sometimes cross-cut by straight burrows that are about 5 mm in diameter and up to 7 cm deep. In two cases, the burrows terminate in a presumed *Barnea* sp. cast (Mollusca: Bivalvia: Pholadidae). There is the suggestion of 1–2 cm thick ‘bedding’ in some samples. Close examination reveals possible low angle cross-laminations within one ‘bed’ while others contain very subtle fining-upwards grading. The laminations in some samples display some gentle undulations that may be due to the draping effect, when manganese precipitate mimics the underlying surface. In other cases, however, it appears to involve soft-sediment deformation. In one instance, folding seems to have commenced as box-folds, with limbs of 2.5 cm long and straight crests connecting the limbs 4 cm long, after which the layering becomes overfolded and the upper limb thrusts out.

Calcareous nannofossils were found in layers in four samples (Fig. 4). In three of them (05–01, 05–02 and 05–03), the nannofossils were found in the basal layer of the manganese encrustation in contact with the underlying rock, while in 05–13 the nannofossils were recovered from the basal layer of the encrustation sample. The presence of *Emiliana huxleyi* in 05–01 indicates the uppermost Pleistocene–Holocene Zone NN21 or the upper part of CNPL11 Zone. The FO of *E. huxleyi* delineates the lower boundary of Zone NN21; the base of the Zone CNPL11 is marked by the LO of *Pseudoemiliana lacunosa*. The absence of *Ps. lacunosa* and the presence of scarce *E. huxleyi* indicate that this sample most probably refers to the upper part of CNPL11 Zone. The dominant species are *Gephyrocapsa oceanica*, *Gephyrocapsa* sp. (medium), *Calcidiscus leptoporus*, *Helicosphaera carteri*, *Reticulofenestra* sp. (small) and *Umbilicosphaera sibogae*.

The other three samples (05–02, 05–03 and 05–13) have moderately preserved nannofossil assemblages (Fig. 4). The dominant species are *Calcidiscus leptoporus*, *Gephyrocapsa caribbeanica* (medium), *Gephyrocapsa* sp. (small) and *Reticulofenestra* sp. (small). *Gephyrocapsa oceanica* (medium) and *Ps. lacunosa* are found in fewer numbers, and *Calcidiscus macintyreii* is rare. The presence of *C. macintyreii* and the absence of *Discoaster brouweri* confirm the assignment of these samples to the lower part of Zone NN19 (lower Pleistocene). According to the zonation of Backman et al. (2012), these samples may be referred to the Zone CNPL8, the base of which is fixed by the base of the *Gephyrocapsa* ($\geq 4 \mu\text{m}$) and the top of *Gephyrocapsa* ($\geq 5.5 \mu\text{m}$). In the lower part of Zone CNPL8 the LO of *C. macintyreii* is recorded (Backman et al. 2012). The ‘medium-sized’ *Gephyrocapsa* which including medium sized *G. caribbeanica* and *G. oceanica* are found in all three samples. The presence of group of medium geophyrocapsid and *C. macintyreii* allows referring these samples to the lower part of the Zone CNPL8 (basal Calabrian).

Dredge locality DL2

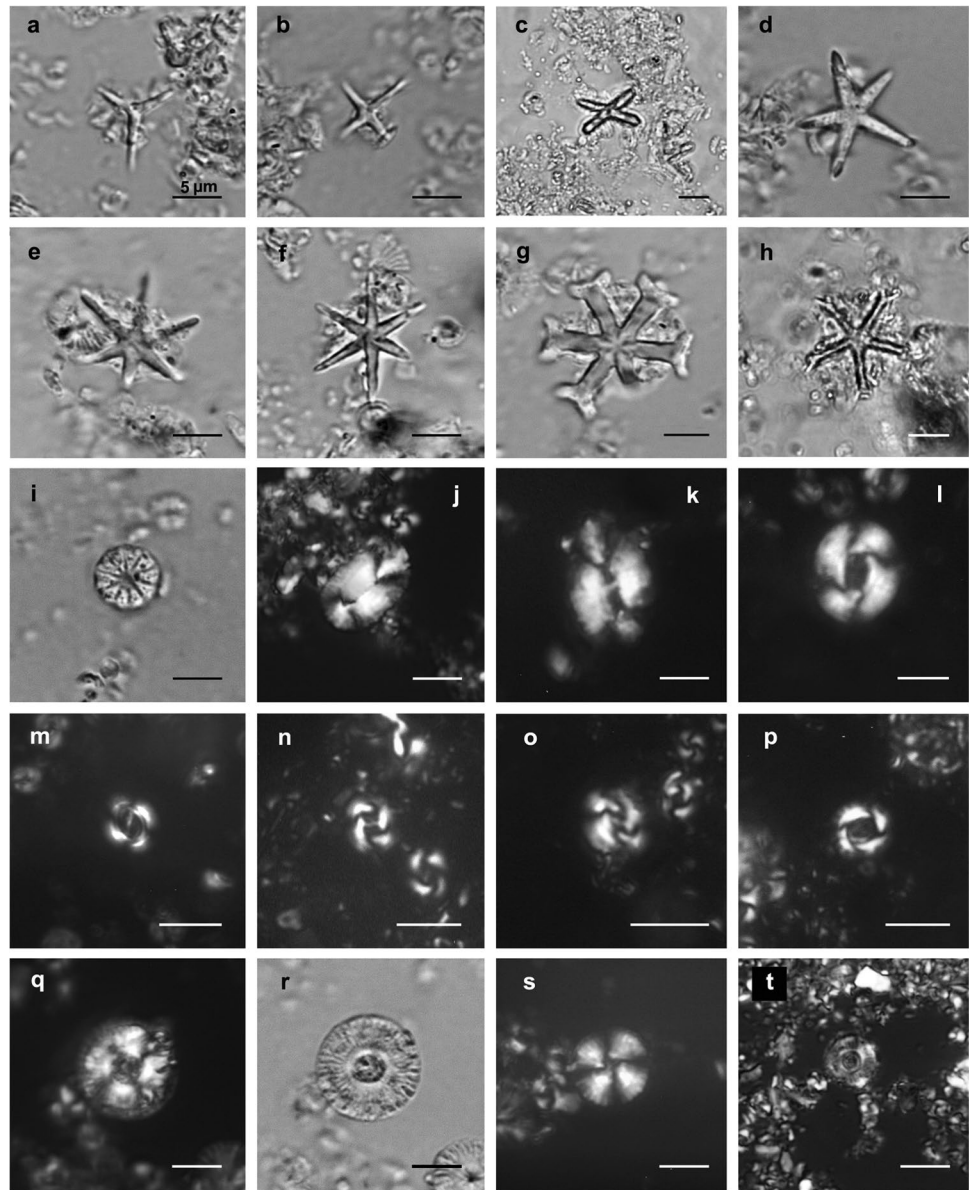
This dredge locality was at the southernmost extremity of the Mozambique Ridge and only yielded a total of seven samples, in each case involving a rock sample encrusted by manganese. In one specimen (05–27), calcareous nannofossils were recovered from the basal layer of the encrustation. The nannofossil preservation is poor, and the uncommon occurrence of *Gephyrocapsa oceanica* allows to place this sample only in a very broad interval of Zones NN19–NN21 or CNPL8–CNPL11, i.e. early Pleistocene–Holocene (Fig. 4). Due to the poor preservation of nannofossils, and therefore unreliable dating, this sample has been excluded from further analysis.

Dredge locality DL3

At this locality, dredging took place on the south-west flank and top of a small hill towards the centre of the southern section of the Mozambique Ridge (Fig. 1; Table 1). All of the rocks recovered were either encrusted in manganese or were fragments of encrustations and nodules. Some were burrowed, bioturbated and contained bivalve remains or their imprints, while two others contained bone fragments. Some samples had contorted laminations. Manganese nodules ranged from 5 to 10 cm diameter and when sectioned, commonly had a calcareous core which, in the larger nodules, was porous and decomposed. This locality provided 15 samples with calcareous nannofossils.

The richest nannofossil assemblages are found in the cores of three samples, all with good preservation (05–34, 05–36 and 05–37) (Fig. 5). The assemblages of these

Fig. 2 Calcareous nannoplankton from the Mozambique Ridge and the Jaguar seamount in the Mozambique Channel. All illustrations are light micrographs. The abbreviations ‘pol’ and ‘tr’ denote polarised and transmitted light, respectively. **a** *Discoaster triradiatus*, sample DL3:05–36, tr; **b** *Discoaster tamalis*, sample DL3:05–36, tr; **c** *Discoaster blackstockae*, sample DL3:05–43, tr; **d** *Discoaster asymmetricus*, sample DL3:05–43, tr; **e** *Discoaster brouweri*, sample DL3:05–36, tr; **f** *Discoaster brouweri*, sample DL3:05–34, tr; **g** *Discoaster pansus*, sample DL3:05–36, tr; **h** *Discoaster pentaradiatus*, sample DL3:05–36, tr; **i** *Hayaster perplexus*, sample DL3:05–34, tr; **j** *Helicosphaera carteri*, sample DL3:05–48, pol; **k** *Helicosphaera sellii*, sample DL3:05–43, pol; **l** *Reticulofenestra pseudoumbilicus*, sample DL3:05–37, pol; **m** *Gephyrocapsa oceanica*, sample DL3:05–55, pol; **n** *Gephyrocapsa parallela*, sample DL3:05–35, pol; **o** *Gephyrocapsa caribbeanica*, sample DL3:05–48, pol; **p** *Pseudoemiliania lacunosa*, sample DL1:05–02, pol; **q** *Calcidiscus macintyreii*, sample DL3:05–43, pol; **r** *C. macintyreii*, sample DL3:05–43, tr; **s** *C. leptoporus*, sample DL3:05–38, pol; **t** *Umbilicosphaera sibogae*, sample DL3:05–38, pol



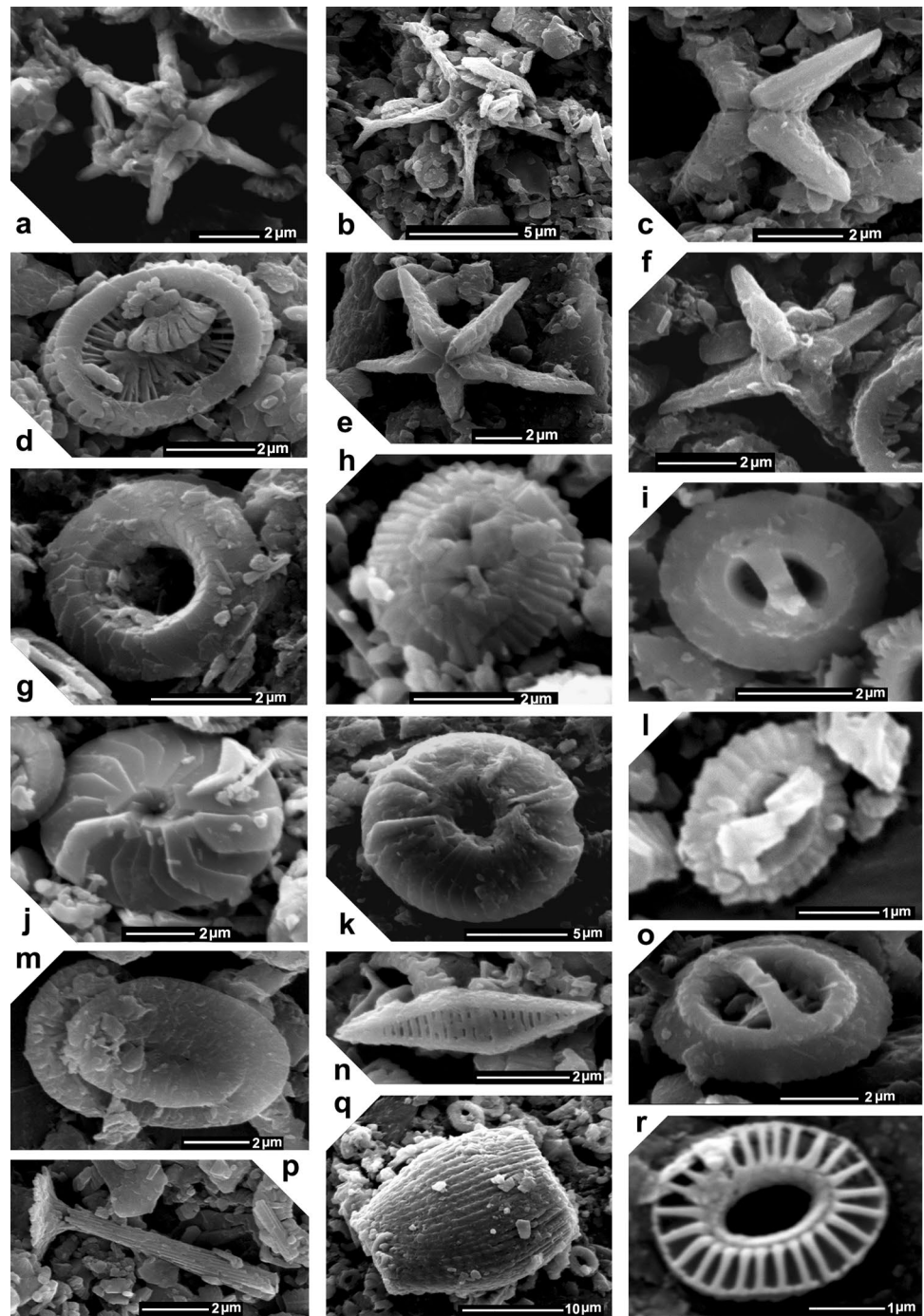
samples are characterised by dominant species *Calcidiscus leptoporus*, *C. macintyreii* and *Coccolithus pelagicus*. *Dicthyococcites* sp., *Discoaster asymmetricus*, *D. deflandrei*, *D. pentaradiatus*, *D. surculus*, *Helicosphaera carteri*, *Pseudoemiliania lacunosa*, *Reticulofenestra pseudoumbilicus*, *Syracosphaera pulchra* and *Umbilicosphaera sibogae* are less common to rare. A rich assemblage of Miocene–Pliocene discoasters has been identified in these samples: *Discoaster brouweri*, *D. pentaradiatus*, *D. surculus*, *D. variabilis*, *D. tamalis* and *D. asymmetricus*. The species *D. tamalis*, *D. asymmetricus*, *Reticulofenestra pseudoumbilicus* and *Pseudoemiliania lacunosa* are stratigraphically most important and present in all three samples, except for *D. tamalis* which is absent from 05–37.

In the sample 05–36, *Discoaster triradiatus* and *Discoaster pansus* have been found. *Discoaster triradiatus* ranges from the upper Miocene (NN9) through terminal Pliocene (top NN18) (Browning et al. 2017). The FO of *Discoaster pansus* is recorded within NN5 (lower/middle Miocene) and its LO is within NN15 (lower/upper Pliocene).

The FO of *Discoaster asymmetricus* delineates the base of Zone NN15 (early/late Pliocene) and disappears within Zone NN18 (upper Pliocene). *Discoaster tamalis* is distributed in a narrow interval. Its FO is recorded within Zone NN14 (lower Pliocene), and its LO is established near the top of Zone NN16 (upper Pliocene).

Reticulofenestra pseudoumbilicus is stratigraphically widely distributed. Its FO is recorded within the Zone NN4

Fig. 3 SEM pictures of calcareous nanoplankton from the samples of the manganese deposits of the Mozambique Ridge and Mozambique Basin. **a** *Discoaster brouweri*, DL3:05–36; **b** *Discoaster pentaradiatus*, DL3:05–43; **c** *Discoaster tamalis*, DL3:05–36; **d** *Syracosphaera pulchra*, proximal view, DL3:05–43; **e** *Discoaster* cf. *asymmetricus*, DL3:05–36; **f** *Discoaster tamalis*, DL3:05–36; **g** *Umbilicosphaera sibogae*, distal view, DL3:05–37; **h** *Gephyrocapsa caribbeanica*, distal view, DL3:05–48; **i** *Gephyrocapsa oceanica*, distal view, DL1:05–01; **j** *Calcidiscus leptoporus*, distal view, DL3:05–48; **k** *Calcidiscus macintyreii*, distal view, DL3:05–36; **l** ‘small’ *Gephyrocapsa* spp., distal view, DL3:05–48; **m** *Helicosphaera carteri*, proximal view, DL3:05–38; **n** *Calciosolenia fossilis*, general appearance, DL1:05–02; **o** ‘large’ *Gephyrocapsa* spp., distal view, DL3:05–38; **p** *Rhabdosphaera claviger*, general appearance, DL3:05–43; **q** *Scyphosphaera* sp., lateral view, DL3:05–36; **r** *Emiliana huxleyi*, distal view, DL1:05–01



(lower Miocene), and its LO is established at the top of Zone NN15 (lower/upper Pliocene). The FO of *Pseudoemiliana lacunosa* is recorded within Zone NN15 (lower/upper Pliocene), and its LO is recorded at the top of Zone NN19 (upper Pleistocene). These samples correspond to Martini's (1971) Zone NN15 (lower/upper Pliocene) due to the presence of *Reticulofenestra pseudumbilicus* and the absence of *Amaurolithus tricorniculatus*. The presence of *D. asymmetricus* and *R. pseudumbilicus* allows referring all three samples to Zone CNPL3 (Backman et al. 2012). *Pseudoemiliana*

lacunosa has been found in all three samples; the presence of this species is fixed in the upper part of CNPL3 Zone. Co-occurrence of *R. pseudumbilicus* and *Ps. lacunosa* indicates that these samples fall into the upper part of Zone CNPL3 (upper Zanclean, lower Pliocene) by Backman et al. (2012).

Sample 05–43, an encrustation with a similarly rich nanofossil assemblage with good preservation, yielded the stratigraphically important yet rare species: *D. asymmetricus*, *D. blackstockae*, *D. pentaradiatus*, *D. surculus*,

interval from the top of *Reticulofenestra pseudoumbilicus* and the top of *D. tamalis*.

Sample 05–52 is an encrustation with a well preserved but very impoverished nannofossil assemblage, which is represented only by *Pseudoemiliana lacunosa*, *Calcidiscus leptoporus* and *Helicosphaera carteri*. The last two species are distributed in a broad stratigraphic range. The FO of *Ps. lacunosa* is recorded within the lower Pliocene Zone NN15 (middle part of CNPL3), while its disappearance demarcates the upper boundary of the middle Pleistocene Zone NN19 (CNPL10). *Reticulofenestra pseudoumbilicus*, which LO marks the upper boundary of NN15 (CNPL3), has not been found in this sample. Sample 05–52 can conditionally be referred to a broad stratigraphic interval of zones NN16 (CNPL4)–NN19 (CNPL10), but is excluded from further analysis due to unreliability of dating.

Five samples (05–53, 05–49, 05–54, 05–48 and 05–42) yielded nannofossils from the lower Pleistocene. Sample 05–49 is an encrustation with moderate preservation, samples 05–42 and 05–54 are cores with moderate preservation and samples 05–53 and 05–48 are cores with good preservation of nannofossils. The dominant species are *Calcidiscus leptoporus* and *Gephyrocapsa caribbeanica* (medium). *Calcidiscus macintyreii*, *Helicosphaera carteri*, *H. sp.*, *Diclyococcites sp.* and *Reticulofenestra sp.* (small) are recorded in low numbers.

The presence of *Calcidiscus macintyreii* and the absence of *D. brouweri* place these samples to the lower part of Zone NN19 (lower Pleistocene). The LO of *D. brouweri* defines the lower boundary of this zone and the LO of *C. macintyreii* is recorded within the lower part of NN19.

According to the zonation of Backman et al. (2012), these samples can be referred to Zone CNPL8, which lower boundary is fixed by the base of *Gephyrocapsa* ($\geq 4 \mu\text{m}$) and upper boundary by the top of *Gephyrocapsa* ($\geq 5.5 \mu\text{m}$). In the lower part of Zone CNPL8, the LO of *C. macintyreii* is recorded (Backman et al. 2012). The group of ‘medium sized’ *Gephyrocapsa*, which includes *G. caribbeanica* and *G. oceanica*, was recorded from almost all five samples. *Gephyrocapsa caribbeanica* was recorded in all samples, and *G. oceanica* was found in samples 05–54, 05–48, 05–49 and 05–42. The presence of the medium *gephyrocapsid* group and *C. macintyreii* allows referring these samples to the lower part of the Zone CNPL8.

The assemblage of samples 05–38 (an interlayer in an encrustation with good preservation) and 05–55 (a core with poor preservation) is characterised by dominant *Calcidiscus leptoporus*, *Gephyrocapsa caribbeanica* (medium), *Pseudoemiliana lacunosa* and *Reticulofenestra sp.* (small). *Gephyrocapsa oceanica* (medium), *Gephyrocapsa sp.* (large), *Helicosphaera carteri* and *H. sellii* are recorded in low quantities. Both samples are placed within the lower part of the lower Pleistocene Zone NN19 by

Martini (1971), based on the presence of *G. caribbeanica* and *H. sellii* and the absence of *Calcidiscus macintyreii*. According to the zonation by Backman et al. (2012), these samples belong to Zone CNPL8, which lower boundary is fixed by the base of *Gephyrocapsa* ($\geq 4 \mu\text{m}$) and upper boundary by the top of *Gephyrocapsa* ($\geq 5.5 \mu\text{m}$). In the latter zonation, the FO of ‘large’ *Gephyrocapsa* is recorded in the middle part of the Zone CNPL8. Thus, the co-occurrence of medium forms of *Gephyrocapsa* (*G. caribbeanica* and *G. oceanica*) and large forms of *Gephyrocapsa* and the presence *Helicosphaera sellii* allow placing these samples in the upper part of CNPL8.

Nannofossil assemblages from two cores (05–40 with good preservation and 05–44 with moderate preservation) and an interlayer (05–35 with good preservation) are all similar. *Calcidiscus leptoporus*, *Gephyrocapsa caribbeanica* (medium), *G. oceanica* (medium), *Gephyrocapsa sp.* (small) and *Reticulofenestra sp.* (small) are the dominant species. All three samples may be assigned to the interval of the upper part of the lower-middle Pleistocene Zone NN19 according to Martini’s (1971) scheme. This is based on the presence of the dominant *Gephyrocapsa caribbeanica* (except in 05–35), the absence of *C. macintyreii* and *Helicosphaera sellii* and the presence of *G. oceanica* and *Ps. lacunosa*, which disappearance demarcates the upper boundary of this zone. According to the zonation of Backman et al. (2012), these samples can be referred to Zone CNPL10, which is defined as the interval between the top absence of *Gephyrocapsa* ($\geq 4 \mu\text{m}$) and the top of *Ps. lacunosa*. The presence abundant ‘medium’ and ‘small’ *Gephyrocapsa spp.* and common *Gephyrocapsa parallela* was recorded in all three samples, which is typical for this zone.

Dredge locality DL4

This site on the Jaguar seamount (Fig. 1; Table 1) was the shallowest dredge locality. It yielded samples of volcanic rocks encased in manganese encrustations. One sample (05-78B) contained a moderately preserved nannofossil assemblage that indicated Zone NN21 or the upper part of CNPL11 Zone (upper Pleistocene–Holocene) due to the presence of *E. huxleyi* (Fig. 4). The FO of *E. huxleyi* delineates the lower boundary of Zone NN21; the base of Zone CNPL11 is marked by the LO of *Ps. lacunosa*. The absence of *Ps. lacunosa* and the presence of rare *E. huxleyi* most probably place this sample into the upper part of CNPL11 Zone. The dominant species are *Gephyrocapsa oceanica*, *Calcidiscus leptoporus*, *Gephyrocapsa sp.* (medium), *Helicosphaera carteri* and *Umbilicosphaera sibogae*.

Discussion

It is important to emphasise that, with only a few exceptions, the identified nannofossils come from the basal layer of the manganese encrustation sample or from the core of nodules. Therefore, they are yielding critical information about ages of encrustations and Fe–Mn oxide precipitation rates. Firstly, the age of nannofossils is established in a particular sample. Secondly, this age marks the maximum age of the onset of conditions favourable to Fe–Mn oxide precipitation in the sample, so the thickness of the layer yields a minimum growth rate.

Overall, the samples fall into three age groups and six subgroups (Fig. 6):

- Pliocene: (1) DL3: 05–34, 05–36, 05–37; (2) DL3: 05–43.
- Pleistocene: (3) DL1: 05–02, 05–03, 05–13; DL3: 05–53, 05–49, 05–54; 05–48, 05–42; (4) DL3: 05–38, 05–55; (5) DL3: 05–35, 05–40, 05–44.
- Pleistocene–Holocene: (6) DL1: 05–01; DL4: 05-78B.

In the absence of isotope chronometry, only broad ages in millions of years can be estimated for each subgroup (Backman et al. 2012; Gradstein et al. 2020).

Pliocene

- (1) DL3: 05–34, 05–36, 05–37 (4.04–3.82 Ma)

Although the presence of *Pseudoemiliana lacunosa* places all three samples in the upper part of Zone CNPL3, Backman et al. (2012) do not provide the exact age for the FO of *Ps. lacunosa*. Thus, we use the age of the lower boundary of Zone CNPL3 (4.04 Ma) in calculation of the minimum Fe–Mn oxide precipitation rate, bearing in mind that the actual minimum rate can be slightly higher.

- (2) DL3: 05–43 (3.82–2.76 Ma)

Backman et al. (2012) discuss the age of the disappearance of *Discoaster tamalis* in the interval of 3.01–2.70 Ma, but accept 2.76 Ma in their scheme.

Pleistocene

- (3) DL1: 05–02, 05–03, 05–13 (1.71–1.60 Ma)

The range of the entire Zone CNPL8 is 1.71–1.25 Ma, but Backman et al. (2012) note that *Calci-*

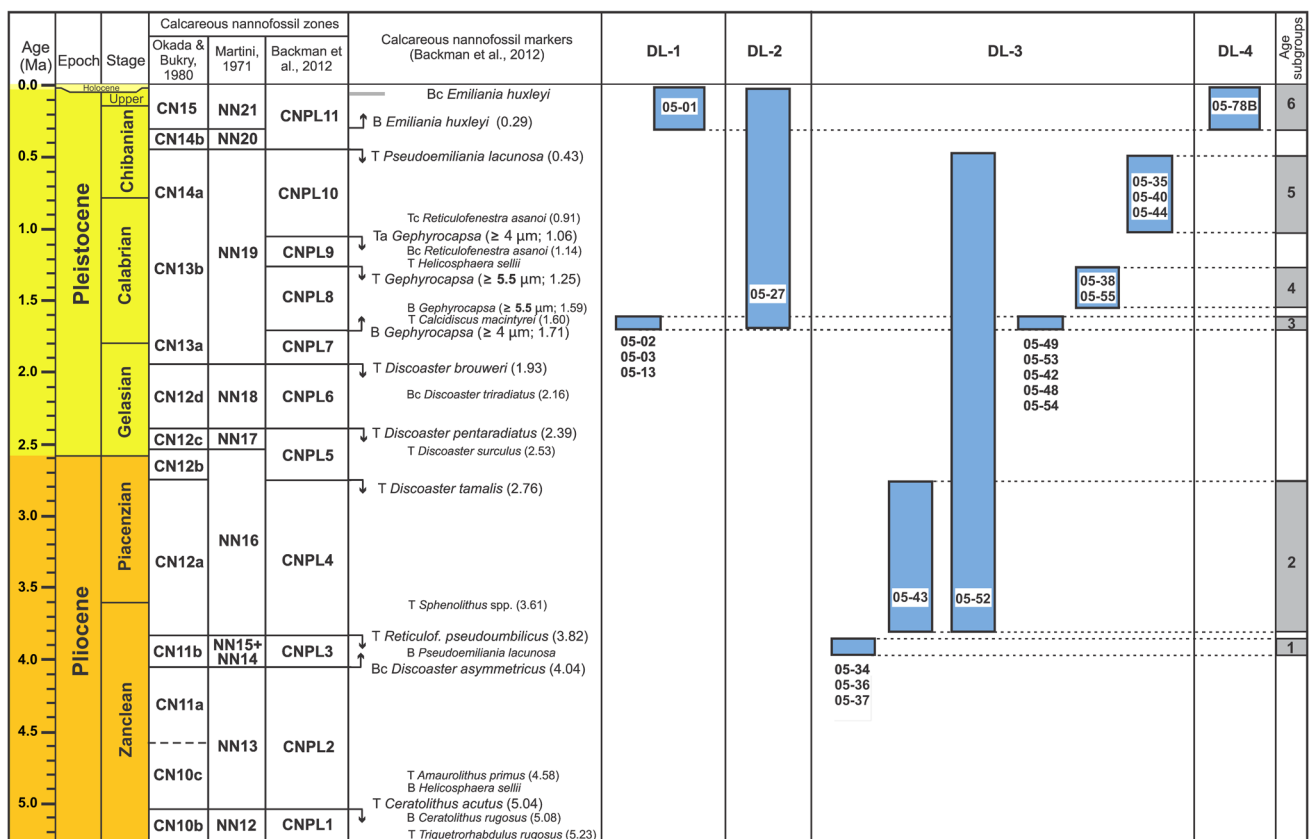


Fig. 6 Calcareous nannofossil biostratigraphic summary of the Pliocene–Holocene on the Mozambique Ridge and Mozambique Basin, showing the bi-modal (Pliocene and middle Pleistocene–Holocene) age distribution for the nannofossils of subgroups 1–2 vs 3–6 (see

‘Discussion’ section). Sample 05–52 can only be referred to a broad stratigraphic interval due to a very impoverished nannofossil assemblage. Pliocene and Pleistocene biozones by Backman et al. (2012)

discus macintyreii disappears in the lower part of the zone (1.60 Ma), just before the appearance of ‘large’ *Gephyrocapsa* spp. ($> 5.5 \mu\text{m}$) at 1.59 Ma. Since we have observed both *C. macintyreii* and ‘medium’ *Gephyrocapsa* spp. ($\geq 4 \mu\text{m}$) in all three samples, we use 1.60 Ma as the upper limit for calculating the minimum Fe–Mn oxide precipitation rate.

- (4) DL3: 05–53, 05–49, 05–54; 05–48, 05–42 (1.71–1.60 Ma)

These samples have also yielded both *C. macintyreii* and ‘medium’ *Gephyrocapsa* spp. ($\geq 4 \mu\text{m}$), so we use 1.60 Ma as the upper limit for calculating the minimum Fe–Mn oxide precipitation rate, as discussed above.

- (5) DL3: 05–38, 05–55 (1.59–1.25 Ma)

Contrary to subgroup 3, samples 05–38 and 05–55 are characterised by the presence of ‘large’ *Gephyrocapsa* spp. ($> 5.5 \mu\text{m}$) and the absence of *C. macintyreii*, so 1.59 Ma is used for calculating the minimum Fe–Mn oxide precipitation rate.

- (6) DL3: 05–35, 05–40, 05–44 (1.06–0.43 Ma)

This age interval corresponds to the entire range of Zone CNPL10.

Pleistocene–Holocene

- (7) DL1: 05–01; DL4: 05-78B (0.29–0.00 Ma)

Both samples contain *Emiliania huxleyi*, which FO is commonly accepted at 0.29 Ma (Backman et al. 2012; Gradstein et al. 2020).

There are several major routes of the Fe–Mn oxide precipitation in the ocean, i.e. hydrogenetic, hydrothermal, mixed hydrogenetic/hydrothermal and diagenetic (Koschinsky and Hein 2017). Each results in considerably differing rates of Fe–Mn oxide accumulation. The hydrogenetic process is the slowest, with only few millimetres per 1 Ma. Thus, for example, for hydrogenous Fe–Mn encrustations, Ingram et al. (1990) reported growth rates of 0.9–5.4 mm/Ma from the Pacific; Eisenhauer et al. (1992) estimated rates of 6.2 mm/Ma in the Quaternary of the Pacific. Usui and Terashima (1997) observed rates of 1.1–2.8 mm/Ma in the NW Pacific, and Frank et al. (2002) identified rates of 0.7–6.14 mm/Ma in different parts of the Atlantic, Southern and Indian oceans. In the SW Atlantic, Benites et al. (2020) calculated growth rates of 0.57–1.39, 2.07–4.31 and 1.48–4.38 mm/Ma using different Co-chronometer equations for non-phosphatized and phosphatized layers. Josso et al. (2020) mentioned rates of between 0.8 and 14 mm/Ma for the NE Atlantic. Most importantly for this study, Charles et al. (2020) noted rates of 1.3–3.6 mm/Ma for the Mozambique Channel, without, however, explaining how these values were obtained.

The hydrothermal route manifests in much higher, sometimes by several orders of magnitude, rates of Fe–Mn oxide precipitation. Ingram et al. (1990) provided rates

of $\geq 33 \text{ mm/Ma}$ for hydrothermally originated encrustations in the Pacific, and Usui and Terashima (1997) suggested rates of up to 1000 mm/Ma for young hydrothermal crusts in the NW Pacific. The mixed hydrogenetic/hydrothermal and diagenetic accumulation is characterised by intermediate growth rates, which, however, never reach extremely high values. Thus, Ingram et al. (1990) suggest Fe–Mn oxide precipitation rates of about 20 mm/Ma in the Pacific, whereas Glasby and Andrews (1978) mentioned 1.5, 3.5–36 and 10–20 mm/Ma while discussing diagenetic processes of accretion on the Hawaii Ridge.

Noteworthy are estimates of Fe–Mn accretion rates based on the calcareous nannofossil biostratigraphy. Cowen et al. (1993) calculated 0.8–2 mm/Ma for different intervals between the Palaeocene/Eocene boundary and lower Pliocene, applying calcareous nannofossil biostratigraphy to a Fe–Mn crust from Hawaii. The authors did not explicitly indicate the geochemical origin of the crust, which, however, can be identified as hydrogenous based on the inferred rate of its accretion.

Harada and Nishida (1976) analysed a Mn nodule dredged at the summit of the Makarov Guyot (depth 1378 m), NW Pacific, and identified calcareous nannofossils from outer and inner surfaces of its layers. The nodule had a 2-mm thick outer, 8-mm thick middle and 50-mm thick innermost layer. The calcareous nannofossil assemblage identified on the inner surface of the outmost layer allowed the authors to attribute the complex to NN19 Zone, for which they accepted the interval of 2–0.5 Ma, and to calculate the growth rate of 1.0–6.7 mm/Ma for this layer. Harada and Nishida identified *Pseudoemiliania lacunosa* and *Calcidiscus macintyreii* among other stratigraphically broadly distributed species in that assemblage. While the presence of the former (and the evident absence of discoasters) justifies the placement of the assemblage to NN19, the latter species disappears in the lower part of CNPL8 Zone at 1.60 Ma according to Backman et al. (2012). This does not affect much the calculation of the minimum growth rate of the outer layer, but has a far-reaching consequence for estimation of the accretion rate of the two inner layers. Harada and Nishida (1976) identified *Gephyrocapsa oceanica* in the innermost layer adjacent to the basaltic nucleus; this, coupled with the absence of *Discoaster* spp., allowed the authors to suggest 2 Ma as the maximum age for the onset of the Mn precipitation and to calculate its minimum rate for the two inner layers as 39 mm/Ma (there is apparently a typo, since the rate should be 29 mm/Ma). However, the new age constraint by *C. macintyreii* from above puts the formation of the two inner layers in the interval of 1.93–1.60 Ma and allows us to calculate a reliable Mn precipitation rate of 176 mm/Ma for the two inner layers. Harada and Nishida (1976) did note that the massive texture of the inner layer was indicative of a rapid (i.e. hydrothermally driven) growth. The West Pacific

Seamount Province is generally characterised by slow (i.e. hydrogenetic) rates of the Fe–Mn oxide precipitation (Okamoto and Usui 2014), but there is evidence of hydrothermal processes of manganese accretion in the region (e.g. Usui and Nishimura 1992; Usui and Terashima 1997).

In terms of the rate of the Fe–Mn oxide precipitation, our material from the Mozambique Ridge falls into three categories. Two samples (05–34 and 05–43, from a core and an encrustation dated back to the Pliocene) show the slowest growth of 6.9–7.3 and 4.7–6.5 mm/Ma (Table 2), respectively; these rates are in agreement with the hydrogenetic processes, although they lie at the upper boundary of ever recorded values for this mode of accretion.

All other samples, save for 05–36, 05–37 and 05–53, demonstrate much higher rates of precipitation between 20.8 and 248.3 mm/Ma (Table 2). This is suggestive of a hydrothermal origin. The remaining three samples (05–36, 05–37 and 05–53), with their calculated growth rates of 9.9–14.4 mm/Ma, may well originate from a mixed hydrogenetic/hydrothermal process.

Overall, the calculated Fe–Mn oxide precipitation rates of 4.7 to 248.3 mm/Ma (Table 2) are indicative of the hydrothermal rather than hydrogenetic origin, contrary to the earlier obtained geochemical data (Perritt and Watkeys 2007). Further to this, manganese precipitation was apparently not continuous. Samples from dredge sites DL1 and DL3 contain older manganese

laminations with burrows that do not continue upwards into the overlying younger laminations. Consequently, there must have been a period of time when the contact between these two series of laminations formed an exposed surface, thus allowing burrowing and, in places, bioturbation to take place prior to manganese precipitation being resumed.

The bi-modal (Pliocene and middle Pleistocene–Holocene) ages for the nannofossils (subgroups 1 and 2 vs 3–6, Fig. 6) probably reflect oceanographic changes in the SW Indian Ocean in response to major global events taking place elsewhere. The mid-Pliocene was the time when the Panama Isthmus finally closed (Lunt et al. 2008). This event caused a reorganisation of the currents in the Atlantic Ocean, resulting in an initial pulse of North Atlantic Deep Water (NADW) into this region of the SW Indian Ocean as attested by an increased isotopic signal around 3–4 Ma (Burton et al. 1997). Precipitation of manganese from the middle Pleistocene to Holocene was probably brought about by onset of the Northern Hemisphere glaciations that influenced the vector and dynamics of the NADW during the Quaternary (Rutberg et al. 2000; Frank et al. 2002; Bell et al. 2015; Bergh et al. 2021). However, more data on nannofossils from Mn nodules from a broader stratigraphic interval preceding the Pliocene and from other localities in SW Indian and SE Atlantic oceans are needed to test this hypothesis.

Reworked calcareous nannofossils are found at all dredge sites except DL2, which is close to the CCD and therefore not conducive to preservation of calcareous microfossils. Despite the small number of species (see Appendix), when taken overall they have been reworked from the Eocene to early Pliocene rocks. These ages correspond to the primarily Palaeocene/Eocene to early Pliocene sequences that have been identified in the Transkei Basin and Natal Valley (Niemi et al. 2000; Schlüter and Uenzelmann-Neben 2007). In addition, dredge sites DL1 and DL3 contain reworked Cretaceous nannofossils. This implies that in the Pliocene and Pleistocene, bottom currents must have eroded the Upper Cretaceous sedimentary sequences (Schlüter and Uenzelmann-Neben 2007).

With regards to the possibility of tectonic activity, the samples from dredge site DL1 contain features typical of soft-sediment deformation. As the Mozambique Ridge is an oceanic structure known to be associated with earthquakes (Craig et al. 2011), it seems likely that these features were formed due to instabilities caused by earthquakes during the Pleistocene. It is known that the axis of earthquake activity started to extend deep into the Natal Valley, following the oceanward propagation of the East African Rift System during the Neogene (Wiles et al. 2014).

Table 2 Calculated growth rates (mm/Ma) based on the average age of nannofossil-dated basal layers in samples

Dredge locality	Sample no	Thickness (mm)	Age of layer (Ma)	Min. growth rate (mm/Ma)
DL1	05–01	72	0.29–0.00	≥ 248.3
DL1	05–02	65	1.71–1.60	38.0–40.6
DL1	05–03	44	1.71–1.60	25.7–27.5
DL1	05–13	57	1.71–1.60	33.3–35.6
DL3	05–34	28	4.04–3.82	6.9–7.3
DL3	05–35	75	1.06–0.43	70.8–174.4
DL3	05–36	55	4.04–3.82	13.6–14.4
DL3	05–37	45	4.04–3.82	11.1–11.8
DL3	05–38	58	1.59–1.25	36.5–46.4
DL3	05–40	45	1.06–0.43	42.5–104.7
DL3	05–42	44	1.71–1.60	25.7–27.5
DL3	05–43	18	3.82–2.76	4.7–6.5
DL3	05–44	26	1.06–0.43	24.5–60.5
DL3	05–48	45	1.71–1.60	26.3–28.1
DL3	05–49	45	1.71–1.60	26.3–28.1
DL3	05–53	17	1.71–1.60	9.9–10.6
DL3	05–54	52	1.71–1.60	30.4–32.5
DL3	05–55	33	1.59–1.25	20.8–26.4
DL4	05–78B	12	0.29–0.00	≥ 41.4

Conclusions

Manganese precipitation on the Mozambique Ridge as nodules during the mid-Pliocene possibly occurred in response to changes in ocean currents that took place when the Panama Isthmus closed and the NADW penetrated the region. A return of the NADW to the region due to the onset of the Quaternary glaciations in the Northern Hemisphere might have caused the precipitation of further manganese deposits as encrustations on the Mozambique Ridge and the Jaguar seamount from the terminal Pleistocene to Holocene. Fluctuations in oceanographic conditions due to glacial and interglacial periods were possibly responsible for the ages of precipitation recorded in this study. On the basis of the calculated growth rates, which are 4.7–248.3 mm/Ma, the manganese deposits are considered mainly hydrothermal in origin.

There is an unfortunate void with respect to detailed geological, palaeontological and palaeoceanographic information in this part of the SW Indian Ocean. The results of this study reveal the potential of the Mozambique Ridge and environs with respect to filling this gap. The samples obtained by dredging indicate that in all probability the Mozambique Ridge has a complete Pleistocene and most likely Tertiary sedimentary record as well. The ridge is aligned N–S, extending from 35°S to 22°S, and ranges in depth from about 700 m to over 4 km. Consequently, it provides a large latitudinal range and depth variations that have preserved a wide range of oceanographic conditions during the Tertiary–Quaternary. Further detailed investigation will result in a better understanding of the palaeoenvironmental history of the region.

Appendix

Taxonomic list of nannofossil species identified in manganese deposits of the Mozambique Ridge and Mozambique Basin.

Calcidiscus leptoporus (Murray et Blackman, 1898) Loeblich et Tappan, 1978.

Calcidiscus macintyreii (Bukry et Bramlette, 1969) Loeblich et Tappan, 1978.

Calciosolenia fossilis (Deflandre in Deflandre & Fert, 1954) Bown in Kennedy et al., 2000.

Ceratolithus sp.

Coccolithus pelagicus (Wallich, 1877) Schiller, 1930.

Dictyococcites sp.

Discoaster asymmetricus Gartner, 1969.

Discoaster blackstockae Bukry, 1973.

Discoaster brouweri Tan, 1927 emend. Bramlette et Riedel, 1954.

Discoaster pansus (Bukry & Percival, 1971) Bukry, 1973.

Discoaster pentaradiatus Tan, 1927 emend. Bramlette et Riedel, 1954.

Discoaster sp.

Discoaster surculus Martini et Bramlette, 1963.

Discoaster tamalis Kamptner, 1967.

Discoaster triradiatus Tan Sin Hok, 1927.

Discoaster variabilis Martini et Bramlette, 1963.

Discosphaera tubifera (Murray et Blackman, 1898) Ostenfeld, 1900.

Emiliania huxleyi (Lohmann, 1902) Hay et Mohler, 1967.

Florisphaera profunda Okada et Honjo, 1973.

Gephyrocapsa caribbeanica Boundreaux et Hay, 1969.

Gephyrocapsa ericsoni McIntyre et Bé, 1967.

Gephyrocapsa oceanica Kamptner, 1943.

Gephyrocapsa parallela Hay et Beaudry 1973.

Gephyrocapsa sp. (large).

Gephyrocapsa sp. (small).

Hayaster perplexus (Bramlette et Riedel, 1954) Bukry, 1973.

Helicosphaera carteri (Wallich, 1877) Kamptner, 1954.

Helicosphaera sellii Bukry et Bramlette, 1969.

Helicosphaera sp.

Helicosphaera wallichii (Lohmann, 1902) Boundreaux et Hay, 1969.

Pontosphaera discopora Schiller, 1925.

Pontosphaera japonica (Takayama, 1967) Nishida, 1971.

Pontosphaera multipora (Kamptner, 1948) Roth, 1970.

Pontosphaera sp.

Pseudoemiliania lacunosa (Kamptner, 1963) Gartner, 1969.

Reticulofenestra pseudoumbilicus (Gartner, 1967) Gartner, 1969.

Reticulofenestra sp.

Reticulofenestra sp. (small).

Rhabdosphaera clavigera Murray et Blackman, 1898.

Rhabdosphaera procera Martini, 1969.

Scyphosphaera amphora Deflandre, 1942.

Scyphosphaera cantharellus Kamptner, 1955.

Scyphosphaera pulcherrima Deflandre, 1942.

Scyphosphaera sp.

Sphenolithus sp.

Syracosphaera pulchra Lohmann, 1902.

Syracosphaera sp.

Thoracosphaera heimii (Lohmann, 1919) Kamptner, 1941.

Thoracosphaera saxea Stradner, 1961.

Umbellosphaera irregularis Paasche in Markali et Paasche, 1955.

Umbilicosphaera rotula (Kamptner, 1956) Varol, 1982.

Umbilicosphaera sibogae (Weber-van Bosse, 1901) Gaarder, 1970.

Reworked species:

Upper Cretaceous:

Cribrosphaerella ehrenbergii (Arkhangelsky, 1912) Deflandre, 1952.

Kamptnerius magnificus Deflandre, 1959.

Prediscosphaera cretacea (Arkhangelsky, 1912) Gartner, 1968.

Eocene–Miocene:

Chiasmolithus grandis (Bramlette et Riedel, 1954) Radomski, 1968 (early–middle Eocene).

Coccolithus miopelagicus Bukry, 1971 (middle–late Miocene).

Discoaster berggrenii Bukry, 1971 (late Miocene).

Discoaster deflandrei Bramlette et Riedel, 1954 (middle Eocene).

Reticulofenestra perplexa (Burns, 1975) Wise, 1983 (early Oligocene–Miocene).

Reticulofenestra umbilica (Levin, 1965) Martini et Ritzkowski, 1968 (middle Eocene–early Oligocene).

Acknowledgements The assistance and discussions with Wilfried Jokat (Senior Scientist, SO-183 cruise) were invaluable. The staff of SEM and Microscopy Units of the University of KwaZulu-Natal (Pietermaritzburg and Westville campuses) is acknowledged for facilitating access to the relevant equipment. The authors are grateful to Kerry Hunter and Igor Muratov (both KwaZulu-Natal Museum, Pietermaritzburg, South Africa) for their help with retrieving some references and general assistance, and to Andrew Green (University of KwaZulu-Natal) and David Watkins (University of Nebraska-Lincoln, USA) for their most helpful comments on an earlier draft of the manuscript. The study was partly funded by the Council for Scientific and Industrial Research, South Africa.

References

- Albarède F, Goldstein SL, Dautel D (1997) The neodymium isotopic composition of manganese nodules from the Southern and Indian oceans, the global oceanic neodymium budget, and their bearing on deep ocean circulation. *Geochim Cosmochim Acta* 61:1277–1291. [https://doi.org/10.1016/S0016-7037\(96\)00404-8](https://doi.org/10.1016/S0016-7037(96)00404-8)
- Backman J, Raffi I, Rio D, Fornaciari E, Pálíke H (2012) Biozonation and biochronology of Miocene through Pleistocene calcareous nannofossils from low and middle latitudes. *Newsl Strat* 45(3):221–244
- Bell D, Jung S, Kroon D, Hodell DA, Lourens LJ, Raymo ME (2015) Atlantic Deep-water response to the Early Pliocene shoaling of the Central American Seaway. *Sci Rep* 5:12252. <https://doi.org/10.1038/srep12252>
- Benites M, Hein JR, Mizell K, Blackburn T, Jovane L (2020) Genesis and evolution of ferromanganese crusts from the summit of Rio Grande Rise, Southwest Atlantic Ocean. *Minerals* 10: 349 <https://doi.org/10.3390/min10040349>
- Bergh EW, von Koslowski R, Compton JS (2021) Variations in deep water masses along the western margin of South Africa, spanning the last two glacial terminations. *Palaeogeogr Palaeoclim Palaeoecol* 562:110148. <https://doi.org/10.1016/j.palaeo.2020.110148>
- Bosman C, Ovechkina M, Uken R (2007) The Aliwal Shoal revisited: new age constraints from nannofossil assemblages. *S Afr J Geol* 110(4):647–653. <https://doi.org/10.2113/gssajg.110.4.647>
- Bown PR (2005) Cenozoic calcareous nannofossil biostratigraphy, ODP Leg 198 Site 1208 (Shatsky Rise, northwest Pacific Ocean). *Proc ODP, Sci Res* 198:1–44. http://www.dp.tamu.edu/publications/198_SR/VOLUME/CHAPTERS/104.pdf
- Browning E, Bergen J, Blair S, Boesiger T, de Kaenel E (2017) Late Miocene to Late Pliocene taxonomy and stratigraphy of the genus *Discoaster* in the circum North Atlantic Basin: Gulf of Mexico and ODP Leg 154. *J Nannoplankton Res* 37(2–3):189–214
- Bukry D (1973) Low-latitude coccolith biostratigraphic zonation. *Initial Rep DSDP* 15:685–703
- Bukry D (1975) Coccolith and silicoflagellate stratigraphy, northwestern Pacific Ocean Deep Sea Drilling Project, Leg 32. *Initial Rep DSDP* 32:677–701
- Burton KW, Ling H-F, O’Nions RK (1997) Closure of the Central American Isthmus and its effect on deep-water formation in the North Atlantic. *Nature* 386(6623):382–385. <https://doi.org/10.1038/386382a0>
- Charles C, Pelleter E, Révillon S, Nonnotte Ph, Jorry SJ, Kluska J-M (2020) Intermediate and deep ocean current circulation in the Mozambique Channel: new insights from ferromanganese crust Nd isotopes. *Mar Geol* 430:106356. <https://doi.org/10.1016/j.margeo.2020.106356>
- Cowen JP, DeCarlo EH, McGee DL (1993) Calcareous nannofossil biostratigraphic dating of a ferromanganese crust from Schumann Seamount. *Mar Geol* 115:289–306
- Craig TJ, Jackson JA, Priestley K, McKenzie D (2011) Earthquake distribution patterns in Africa: their relationship to variations in lithospheric and geological structure, and their rheological implications. *Geophys J Int* 185:403–434. <https://doi.org/10.1111/j.1365-246X.2011.04950.x>
- Eisenhauer A, Gögen K, Pernicka E, Mangini A (1992) Climatic influences on the growth rates of Mn crusts during the Late Quaternary. *Earth Planetary Sci Lett* 109(1–2):25–36. [https://doi.org/10.1016/0012-821X\(92\)90071-3](https://doi.org/10.1016/0012-821X(92)90071-3)
- Frank M, Whiteley N, Kasten S, Hein JR, O’Nions K (2002) North Atlantic Deep Water export to the Southern Ocean over the past 14 Myr: evidence from Nd and Pb isotopes in ferromanganese crusts. *Paleoceanogr* 17(2):1022. <https://doi.org/10.1029/2000PA000606>
- Glasby GP, Andrews JE (1978) Manganese crusts and nodules from the Hawaiian Ridge. *Pacific Sci* 31(4):363–379
- Gradstein FM, Ogg JG, Schmitz MD, Ogg GM (2020) *Geologic time scale 2020*. 1st ed. Elsevier. <https://doi.org/10.1016/C2020-1-02369-3>
- Green A, Ovechkina MN, Uken R (2008) Nannofossil age constraints for the northern KwaZulu-Natal shelf edge wedge: implications for continental margin dynamics, South Africa SW Indian Ocean. *Cont Shelf Res* 28(17):2442–2449. <https://doi.org/10.1016/j.csr.2008.06.007>
- Harada K, Nishida S (1976) Biostratigraphy of some marine manganese nodules. *Nature* 260(5554):770–771. <https://doi.org/10.1038/260770a0>
- Hein JR, Mizell K, Koschinsky A, Conrad TA (2013) Deep-ocean mineral deposits as a source of critical metals for high- and green-technology applications: comparison with land-based resources. *Ore Geol Rev* 51:1–14. <https://doi.org/10.1016/j.oregeorev.2012.12.001>
- Ingram BL, Hein FR, Farmer GL (1990) Age determinations and growth rates of Pacific ferromanganese deposits using strontium

- isotopes. *Geochem Cosmochem Acta* 54(6):1709–1721. [https://doi.org/10.1016/0016-7037\(90\)90402-7](https://doi.org/10.1016/0016-7037(90)90402-7)
- Janin M-Ch (1985) Biostratigraphie de concretions polymetalliques de l'Archipel des Touamotou, fondee sur les nannofossiles calcaires. *Bull Soc géol France, ser. 8* 1(1):79–87
- Janin M-Ch (1987) The imprints of Cenozoic calcareous nannofossils from polymetallic concretions: biostratigraphic significance for two crusts from the Central Pacific (Line Islands Ridge and Mid-Pacific Mountains). *Abh Geol B-A* 39:121–141. https://www.zobodat.at/pdf/AbhGeolBA_39_0121-0141.pdf
- Jiang X-D, Sun X-M, Guan Y (2019) Biogenic mineralization in the ferromanganese nodules and crusts from the South China Sea. *J Asian Earth Sci* 171:46–59. <https://doi.org/10.1016/j.jseaes.2017.07.050>
- Jokat W, editor (2006) Southeastern Atlantic and southwestern Indian Ocean: reconstruction of the sedimentary and tectonic development since the Cretaceous AISTEK-II: Mozambique Ridge and Mozambique Basin. *Ber Polar- Meeresforsch* 521:1–69
- Josso P, Parkinson I, Horstwood M, Lusty P, Chenery S, Murton B (2019) Improving confidence in ferromanganese crust age models: a composite geochemical approach. *Chem Geol* 513:108–119. <https://doi.org/10.1016/j.chemgeo.2019.03.003>
- Josso P, Horstwood MSA, Millar IL, Pashley V, Lusty PAJ, Murton B (2020) Development of a correlated Fe-Mn crust stratigraphy using Pb and Nd isotopes and its application to paleoceanographic reconstruction in the Atlantic. *Paleoceanogr Paleoclim* 35:e2020PA003928. <https://doi.org/10.1029/2020PA003928>
- König M, Jokat W (2010) Advanced insights into magmatism and volcanism of the Mozambique Ridge and Mozambique Basin in the view of new potential field data. *Geoph J Intern* 180(1):158–180. <https://doi.org/10.1111/j.1365-246X.2009.04433.x>
- Koschinsky A, Hein JR (2017) Marine ferromanganese encrustations: archives of changing oceans. *Elements* 13:177–182. <https://doi.org/10.2113/gselements.13.3.177>
- Lunt DJ, Valdes PJ, Haywood A, Rutt IC (2008) Closure of the Panama Seaway during the Pliocene: implications for climate and Northern Hemisphere glaciation. *Clim Dyn* 30:1–18. <https://doi.org/10.1007/s00382-007-0265-6>
- Martini E (1971) Standard Tertiary and Quarternary calcareous nannoplankton zonation. In: Farinacci A (ed) *Proc. II Planktonic Conf, Roma, 1970*. 2:739–785
- Niemi TM, Ben-Avraham Z, Hartnady ChJH, Reznikov M (2000) Post-Eocene seismic stratigraphy of the deep ocean basin adjacent to the southeast African continental margin: a record of geostrophic bottom current systems. *Mar Geol* 162:237–258. [https://doi.org/10.1016/S0025-3227\(99\)00062-6](https://doi.org/10.1016/S0025-3227(99)00062-6)
- Okada H, Bukry D (1980) Supplementary modification and introduction of code numbers to the low-latitude coccolith biostratigraphic zonation (Bukry, 1973; 1975). *Mar Micropal* 5:321–325
- Okamoto N, Usui A (2014) Regional distribution of Co-rich ferromanganese crusts and evolution of the seamounts in the Northwestern Pacific. *Mar Geores Geotech* 32(3):187–206. <https://doi.org/10.1080/1064119X.2013.877110>
- Ovechkina MN, Watkeys MK, Kretzinger W (2009) Nannoplankton in the manganese deposits of the Mozambique Ridge and Mozambique Basin, southwestern Indian Ocean. *Palaeontol Afr* 44:126–128
- Perritt SM, Watkeys MK (2007) The effects of environmental controls on the metal content in ferromanganese encrustations and nodules from the Mozambique Ridge and in the Mozambique Basin, southwestern Indian Ocean. *S Afr J Geol* 110(2–3):295–310. <https://doi.org/10.2113/gssajg.110.2-3.295>
- Perch-Nielsen K (1985) Cenozoic calcareous nannofossils. In: Bolli HM, Saunders JB, Perch-Nielsen K (eds) *Plankton stratigraphy*. Cambridge Univ. Press, Cambridge, pp 427–554
- Rio D, Fornaciari E, Raffi I (1990) Late Oligocene through early Pleistocene calcareous nannofossils from western equatorial Indian Ocean (Leg 115). *Proc ODP, Sci Res* 115:175–235
- Rogers J (1995) A comparative study of manganese nodules off southern Africa. *S Afr J Geol* 98(2):208–216. <https://hdl.handle.net/10520/EJC-92a096b00>
- Rutberg RL, Hemming SR, Goldstein SL (2000) Reduced North Atlantic Deep Water flux to the glacial Southern Ocean inferred from neodymium isotope ratios. *Nature* 405:935–938. <https://doi.org/10.1038/35016049>
- Sato T, Takayama T (1992) A stratigraphically significant new species of the calcareous nannofossil *Reticulofenestra asanoi*. In: Ishizaki K, Saito T (eds) *Centenary of Japanese micropaleontology*. Terra Sci Publ Company, Tokyo, pp 457–460
- Schlüter Ph, Uenzelmann-Neben G (2007) Seismostratigraphic analysis of the Transkei Basin: a history of deep sea current controlled sedimentation. *Mar Geol* 240:99–111. <https://doi.org/10.1016/j.margeo.2007.02.015>
- Shkolnik EL, Zhegallo EA, Baturin GN, Bogatyrev BA, Gaber M, Gerasimenko LM, Golovin DI, Eganov EA, Elen S, Leiming Y, Kovalenker VA, Kruglyakov VV, Kuleshov VN, Machabeli GA, Melnikov MF, Novikov VM, Orleansky VK, Pakhnevich AV, Slukin AD, Khamkhadze NI, Sharkov AA, Yubko VM (2012) Investigation of manganese and ferro-manganese mineralization in different natural environments by methods of scanning electron microscopy. *Eslan, Moscow*
- Usui A, Nishimura A (1992) Submersible observations of hydrothermal manganese deposits on the Kaikata Seamount, Izu-Ogasawara (Bonin) Arc. *Mar Geol* 106(3–4):203–216. [https://doi.org/10.1016/0025-3227\(92\)90130-A](https://doi.org/10.1016/0025-3227(92)90130-A)
- Usui A, Terashima Sh (1997) Deposition of hydrogenetic and hydrothermal manganese minerals in the Ogasawara (Bonin) Arc Area. *Northwest Pacific Mar Geores Geotech* 15(2):127–154. <https://doi.org/10.1080/10641199709379941>
- Wang X, Müller WEG (2009) Marine biominerals: perspectives and challenges for polymetallic nodules and crusts. *Trends Biotech* 27(6):375–383. <https://doi.org/10.1016/j.tibtech.2009.03.004>
- Wang X, Peine F, Schmidt A, Schröder HC, Wiens M, Schloßmacher U, Müller WEG (2011) Concept of biogenic ferromanganese crust formation: coccoliths as bio-seeds in crusts from Central Atlantic Ocean (Senghor Seamount/Cape Verde). *Nat Prod Comm* 6(5):679–688. <https://doi.org/10.1177/1934578X1100600522>
- Watkeys MK, Brayshaw M, Thackeray Z (2006) *Geology – dredge report*. *Ber Polar- Meeresforsch* 521(23–35):52–54
- Wiles E, Green A, Watkeys M, Jokat W, Krocker R (2014) Anomalous seafloor mounds in the northern Natal Valley, southwest Indian Ocean: implications for the East African Rift System. *Tectonophysics* 630:300–312. <https://doi.org/10.1016/j.tecto.2014.05.030>
- Young JR, Bown PR (1997) Cenozoic calcareous nannoplankton classification. *J Nannoplankton Res* 19:36–47
- Young JR, Bown PR, Lees JA, editors (2017) *Nannotax3 website*. International Nannoplankton Association, 20 Jan 2017. <http://www.mikrotax.org/Nannotax3>

Publisher's note Springer Nature remains neutral with regard to jurisdictional claims in published maps and institutional affiliations.